

Ir-Ni based mono and bimetallic nanocrystals: synthesis, characterization and effect of cationic, anionic, and non-ionic stabilizers

Anjali Goel^a, Shikha^{a*}, Shivani^a and Sudha Tomar^a

^aDepartment of Chemistry, KGC, Gurukul Kangri University, Haridwar 249407, India

CHRONICLE

Article history:
Received October 12, 2020
Received in revised form
November 30, 2020
Accepted January 15, 2021
Available online
January 15, 2021

Keywords:
Iridium
Nickel
Ethylene Glycol
Bimetallic Nanoparticles

ABSTRACT

Nickel based bimetallic nanocrystals, iridium-nickel play an imperative role in catalysis, electrocatalysis, and magnetic applications. In the present work Ir-Ni bimetallic nanoalloys were synthesized by modified polyol reduction method with different cationic, anionic, and non-ionic surface active agents like CTAB, SDS, TSC, and PVP. The non-ionic surface active agent PVP produced a better effect on nanoparticle size than cationic and anionic surfactants. The synthesized bimetallic nanocrystals were characterized by UV-Vis, XRD, FTIR, FESEM, and HRTEM techniques. XRD and FTIR verify the nature of synthesized bimetallic nanocrystals and the interaction between stabilizers and nanoparticles. HRTEM studies reveal that the PVP stabilized Ir-Ni (3:1) and Ir-Ni (1:1) bimetallic nanocrystals are small in size and less dispersed. Particle size range of these nanoparticles is from (1.77-2.36) nm. FESEM images show that nanoparticles are in quasi spherical shape. EDX analysis indicates that the resultant particles are core shell structure with Ni core and Ir shell.

© 2021 Growing Science Ltd. All rights reserved.

1. Introduction

Nanoparticles are the nanometer-sized sturdy particles, negotiated at atomic or molecular scale, to perform either novel or superior physical properties that are not feasible by conventional bulk solids. In the last several years nanotechnology, has evolved as a cutting edge technology interdisciplinary with physical science, biology, chemical science, medicine and material science.¹ Nanocrystals have been enterprise in populous consumer merchandise such as in sunblocker, superficial, paint, implements, computer devices etc.² Transition metal nanocrystals are known to be constructive catalysts for chemical alterations due to their large surface area.³ Iridium is the part of platinum family and used as energizer due to its mercurial oxidation states. It is known as the most erosion resistant component even at temperatures as high as 2000°C. Erosion and heat resistant peculiarities of iridium make it much more lucrative element for alloying aspiration.⁴ Its composites were first inspected for their antineoplastic activity shortly after the disclosure of cis platin.⁵ It is eminent for boosting olefin, aldehyde, and ketone hydrogenation with more reactions viable when used in bimettallism.⁶ Nickel is a imperative passage metal.⁷ Goodman et al. found that the catalytic action of Ni activator was marginally inferior to that of ruthenium, iridium, and rhodium based promoters.⁸ It is the preferred nanocatalyst for numerous reactions owing to its life, immense activity, and relatively economical price.⁹ Specially,

* Corresponding author. Tel.: +91-9465829823
E-mail address: shikhatomar348@gmail.com (Shikha)

the Ir-Ni system was depicted for hydrogen formation by electrocatalytic water splitting or by catalytic hydrazine disintegration as well as for catalytic hydrogen oxidation reactions and for ring opening reactions.¹⁰

Bimetallic nanocrystals (BMNPs) are of massive significance by virtue of the alteration of properties examined, correlated with monometallics, not only due to size effects, but also as an outcome of the merger of various metals.¹¹ Literally, through bimetallication the catalytic attributes of the resulting nanocrystals can be upgraded to great extent which cannot be attained by the use of monometallic energizers. In bimetallic promoters, the photoelectric impact plays an important role which defines the charge alteration.¹² Numerous preparedness techniques of the nanocrystals such as electrolysis, polyol reduction, citrate reduction, Y ray irradiation, organometallic methods, and sol-gel techniques have been nominated.¹³ In all these techniques, polyol reduction is prevalent and auspicious technique for the fusion of Ir-Ni BMNPs.¹⁴

Bimetallic nanocomposites have a thermodynamic propensity to aggregate.¹⁵ Agglomeration has lethal effects such as deferment in ignition and partial combustion of the particles as vigorous, substantial.¹⁶ Therefore surface active agents are used for the kinetic control of nanocrystals shape, morphology, and size.¹⁷

Surface active agents or stabilizers automatically diminish the particle size without altering the structure and reducing ability depending on the type of surfactants.¹⁸ Surface active agents can be determined according to the charge exist in the hydrophilic part of the fragment i.e. cationic, anionic, amphoteric, and non-ionic surfactants.¹⁹ Cetyltrimethylammonium bromide is a cationic surfactant,²⁰ which works as to regulate the phase structure and morphology of the product.²¹ Sodium dodecyl sulphate is an anionic surface active agent and used as homecleansers, in shampoos and in dentifrices.²² Tri sodium citrate is also an anionic surface active agent and it concedes easy growing and lowering the interfacial tension of the solvent.²³ Polyvinylpyrrolidone is a non-ionic surface active agent.²⁴ It is harmless and solvable in many polar solvents. PVP stabilized native metal nanocrystals have widely been used as stimulant for numerous reactions.²⁵

Ethylene glycol is the uncomplicated diol. It is thoroughly mixable with numerous polar solvents and only marginally miscible in non-polar solvents.²⁶ It performs as both solvent and reductive agent.²⁷ In the present work, we have synthesized Ir-Ni bimetallic nanocrystals with (3:1), (1:3), and (1:1) ratios by polyol reduction method, using cationic (CTAB), anionic (SDS, TSC) and non-ionic (PVP) capping agents. These particles were explored using UV-Visible, XRD, FESEM, HRTEM, FTIR methods of analysis.

2. Results and Discussion

2.1. UV-Vis spectrophotometry

The UV-Vis spectra were measured after the reduction of metal ions to form nanocrystals using ethylene glycol as a reference solution. The absorption spectra of Ir, Ni monometallic (MNPs) and Ir-Ni bimetallic nanocrystals in different molar ratios (1:1, 3:1, and 1:3) using different surface active agents PVP, CTAB, SDS, and TSC are shown in **Fig. 1(A)**, **1(B)**, **1(C)**, and **1(D)**. As can be seen in **Fig. 1(A)** that the absorption peaks of precursor salt of (**a**) Ir(III)/PVP, (**b**) Ir(III)/SDS, (**c**) Ir(III)/CTAB, and (**d**) Ir(III)/TSC stabilized are 234nm, 239nm, 330nm, and 236.8nm respectively which on reduction by alcohol shifted to 358nm, 362.2nm, 391nm, and 356.8nm respectively. The shifted peaks are stable and indicate the formation of Ir/surfactant assisted nanocrystals.²⁸ The characteristic peaks of initial mixture of Ni(II)/surfactants CTAB, SDS, TSC, and PVP are 395.2nm, 390.4nm, 383.2nm, and 330nm respectively. These peaks are disappeared in **Fig. 1(B)** and new stable peaks are observed in (**a**, **b**, **c**, and **d**) at 361.6nm, 366.4nm, 359.2nm, and at 412nm for Ni/surfactant i.e. CTAB, SDS, TSC, and PVP supported nanocrystals respectively.⁹ The color of the solution changes from greenish yellow to pale

brown. Color change of the solution also indicates the reduction of metal ions and formation of new species.

Two characteristic peaks are expected for a physical combination of Ir and Ni monometallic nanoparticles (MNPs) but presence of only one new absorption peak in **Fig. 1(C)**and **1(D)** represents clearly the formation of Ir-Ni BMNPs. The characteristic peaks of Ir-Ni (1:1) BMNPs are shown in **Fig. 1(C)**. The absorption band of Ir-Ni/surfactant- SDS, CTAB, PVP, and TSC stabilized BMNPs in **(a, b, c, and d)** are observed at 390.4nm, 560.8nm, 358.4nm, and 368.8nm respectively. The absorption spectra of Ir-Ni (3:1,&1:3) BMNPs are shown in **Fig. 1(D)**. In the spectra **(a, b, c, d, and e)** the formation of new absorption peaks at 376nm, 361.6nm, 558.4nm, 395nm and 371nm for Ir-Ni (3:1) and Ir-Ni (1:3), respectively, represent the formation of BMNPs. The color of the solution turned from pale yellow to blackish brown. Maximum absorption band shifting from monometallic Ir and Ni characteristic peaks depends upon their molar ratios i.e. for Ir-Ni (3:1) shows more shifting than Ir-Ni (1:3) BMNPs.

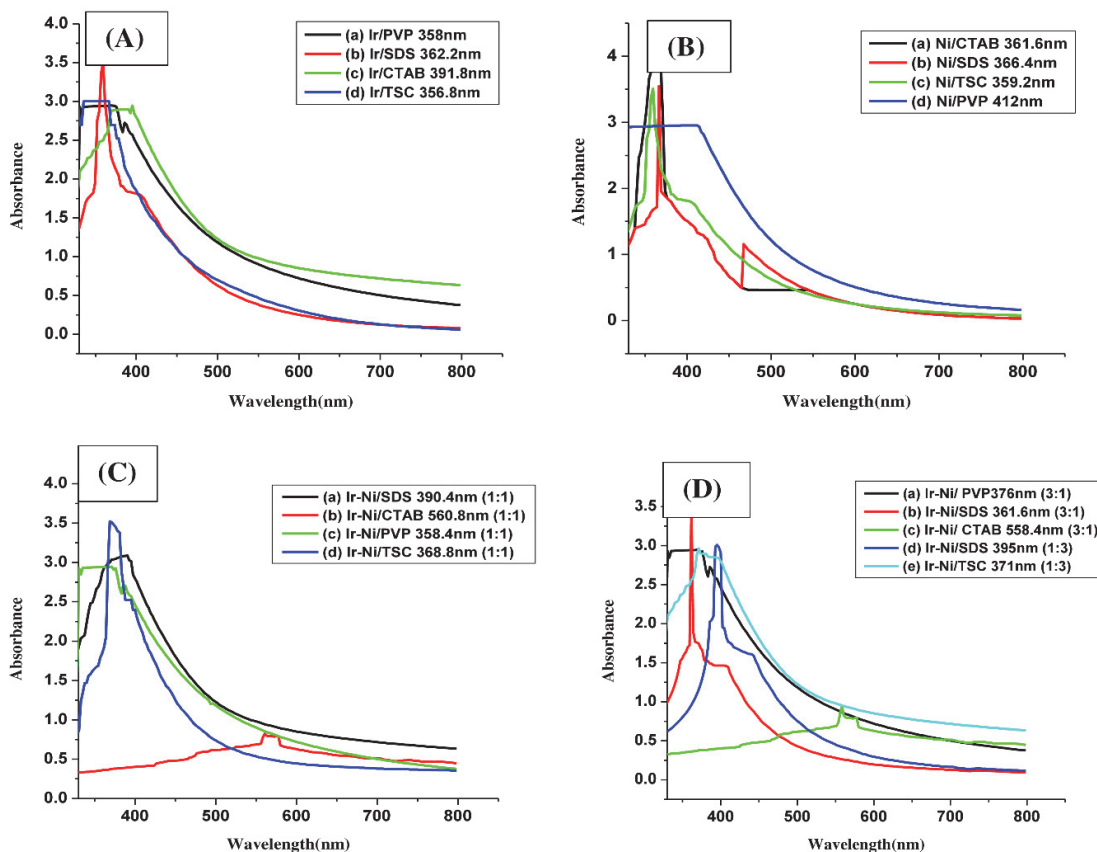


Fig. 1. UV-Vis spectra of (A) Ir MNPs formation (B) Ni MNPs formation (C)Ir-Ni (1:1) BMNPs (D) Ir-Ni (3:1, and 1:3) BMNPs by using different surfactants CTAB, PVP, SDS, and TSC.

2.2. FT-IR (Fourier transform infrared) spectroscopy

FT-IR characterization technique is used to identify the functional groups or molecules present in solvent and surfactant to examine their probable involvement in the synthesis of Ir-Ni/BMNPs.²⁹ **Fig. 2** shows the FTIR spectrum of (A) Ir-Ni (3:1)/PVP and (B) Ir-Ni (1:1)/PVP-BMNPs using ethylene glycol as solvent. Major peaks from FTIR spectra are selected. It was observed that pure PVP shows a strong band at 1687cm^{-1} which is due to the presence of amide $>\text{C}=\text{O}$ group.^{30,31} On comparing the spectra of (A) Ir-Ni (3:1) and (B) Ir-Ni (1:1) BMNPs shifting of frequencies from 3432 to 3430 cm^{-1}

¹are observed which suggesting the N-H stretching vibration of primary and secondary amines and amides respectively. Furthermore, a shift from 1644 to 1641cm⁻¹ and 1104 to 1095cm⁻¹ may assigned to the C=O stretching and C-O stretching of secondary alcohol respectively.³² From this study it is clear that the functional group like N-H, C=O, and C-O are present in PVP and ethylene glycol which could possibly may stabilize and reduce the synthesized Ir-Ni BMNPs in the mixture.

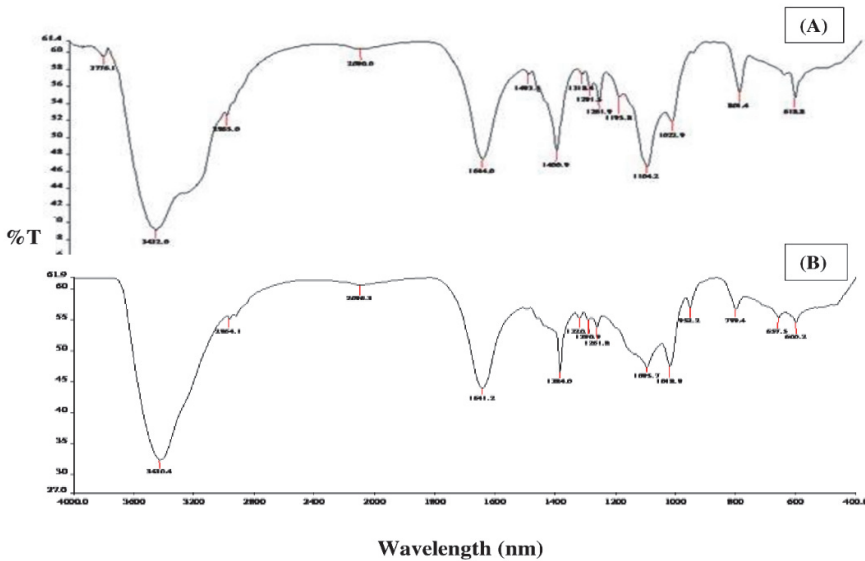


Fig. 2. FT-IR spectra of (A) Ir-Ni (3:1)/PVP and (B) Ir-Ni (1:1)/PVP-BMNPs.

2.3. XRD (*X-ray diffraction*) analysis

Crystallinity and different phases of nanocrystals were identified by X-ray diffraction analysis.³³. The average particle size was calculated using Debye Scherrer equation-

$$D_C = \frac{K\lambda}{\beta \cos \theta},$$

where D_C is the average crystallite size, β is the full width of the observed diffraction peak at its half maximum intensity (FWHM), K is the shape factor which takes a value of about 0.9 and λ is the radiation wavelength which takes a value 0.154nm and θ is the Bragg angle.³⁴ The XRD spectrum of Ir, Ni monometallic nanocrystals and Ir-Ni BMNPs are shown in **Fig. 3**. **Fig. 3(A)** shows XRD spectrum of Ir MNPs using different surfactants PVP, CTAB, SDS, and TSC. XRD spectrum of Ir MNPs between 2θ of 18° - 60° is shown in **Fig. 3(A)**.

The XRD spectra of (a) Ir/PVP stabilized nano shows three peaks at 2θ about 20° , 28° , and 40° . The peaks at 28° and 40° in image (a) are shifted to 26° and at 40° in image (b) Ir/CTAB stabilized nano. In image (c) Ir /SDS stabilized nano shows peak at 2θ about 28° . TSC stabilized Ir-nano in image (d) shows three diffraction peaks at 2θ about 28° , 33° , and 41° respectively. Broad peaks at about 28° , 33° , and 40° show reflection planes (110), (101), and (200) respectively which are characteristics of isolated IrO_2 nanocrystals.³⁵ The diffraction broad peaks also show the amorphous nature of the sample.³⁶ XRD spectra of Ni MNPs using different surface active agents are shown in **Fig. 3(B)**. Two diffraction peaks of Ni/surfactant MNPs with PVP and CTAB [in image (a), and (b)] occur at 2θ values of 37.2° and 43.3° corresponding to (111) and (200) planes respectively. This clearly indicates that the resultant nanocrystals are in NiO form and represent FCC structure. Shifting of these diffraction peaks occurred at 2θ about 44.2° and 51.7° in Ni/surfactants (SDS, & TSC) stabilized MNPs [in image (c), and (d)] corresponding to (111) and (200) planes respectively. XRD spectra of Ir-Ni (1:1) BMNPs using different surfactants are shown in **Fig. 3(C)**. Ir-Ni/ surfactants (PVP, & CTAB) stabilized BMNPs [in

image (a), and (b)] show two diffraction peaks at 2θ about 29.5° and 41.5° respectively and Ir-Ni/surfactants (SDS, & TSC) stabilized BMNPs show diffraction peaks at 2θ about 29.2° , and 43.2° in image (c) and at 33.5° , and 46.6° in image (d). On comparing with the peak of Ir MNPs the diffraction peaks of Ir-Ni BMNPs shift slightly to higher 2θ values thus verifying that the Ni has entered into the Ir lattice forming Ir-Ni alloy form.³⁷XRD spectrum of Ir-Ni (3:1) BMNPs using different surfactants i.e. PVP, CTAB, SDS, and TSC is shown in Fig. 3(D). The diffraction peak of Ir-Ni (3:1) bimetals in image (a), (b), (c), and (d) were observed at 2θ about 28° and 40° which is towards Ir monometals due to high concentration of Ir.³²The diffraction peaks for synthesized Ir-Ni nanocrystals lie between the characteristic peaks of Ir and Ni monometals thus verifying the viable formation of metal alloy or core shell structure.³⁸Synthesis condition and the size of particles calculated by Scherrer equation are given in Tables 1-4. Ir-Ni/ PVP stabilized BMNPs are small in size (< 10 nm) in comparison of CTAB, SDS, and TSC stabilized nanoparticles. As we know that nanoparticles are of great importance due to their small size. Thus, only PVP stabilized particles are considered for HRTEM and FESEM analysis.

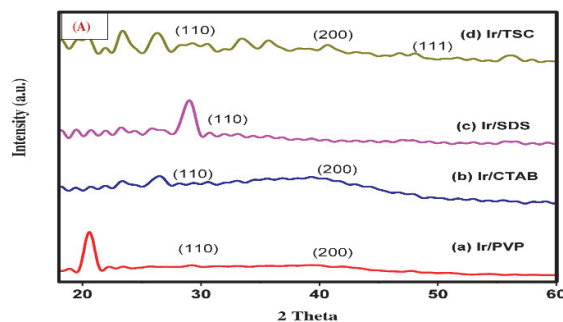


Fig. 3(A). XRD pattern of Ir MNPs using different surfactants

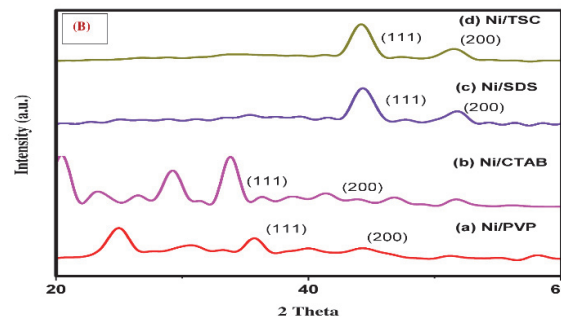


Fig. 3(B). XRD pattern of Ni MNPs using different surfactants

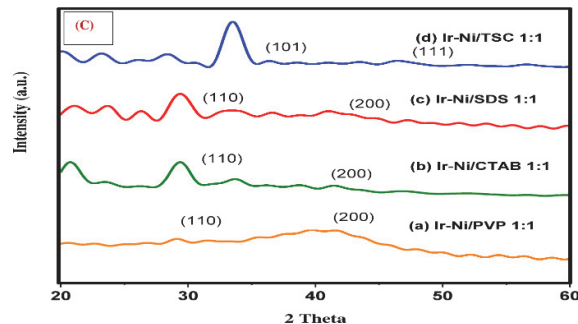


Fig. 3(C). XRD pattern of Ir-Ni (1:1) BMNPs using different surfactants

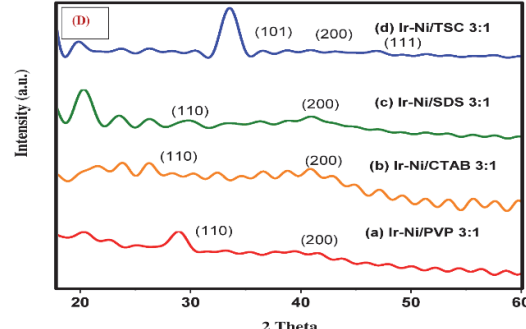


Fig. 3(D). XRD pattern of Ir-Ni (3:1) BMNPs using different surfactants

Table. 1. Synthesis conditions and particle size of Ir-Ni BMNPs with PVP

S. No.	Precursor	Ratio of precursors (%)	Solvent	Surfactant	Approx. particle size in (nm) by XRD
1	IrCl ₃ .3H ₂ O and NiCl ₂ .6H ₂ O	100 : 0.0	Ethylene glycol	PVP	13.6
2	IrCl ₃ .3H ₂ O and NiCl ₂ .6H ₂ O	75:25	Ethylene glycol	PVP	4.8
3	IrCl ₃ .3H ₂ O and NiCl ₂ .6H ₂ O	50:50	Ethylene glycol	PVP	0.8
4	NiCl ₂ .6H ₂ O and IrCl ₃ .3H ₂ O	100:0.0	Ethylene glycol	PVP	26.5

Table. 2. Synthesis conditions and particle size of Ir-Ni BMNPs with CTAB

S. No.	Precursor	Ratio of precursors (%)	Solvent	Surfactant	Approx. particle size in (nm) by XRD
1	IrCl ₃ .3H ₂ O and NiCl ₂ .6H ₂ O	100 : 0.0	Ethylene glycol	CTAB	54.3
2	IrCl ₃ .3H ₂ O and NiCl ₂ .6H ₂ O	75:25	Ethylene glycol	CTAB	33.5
3	IrCl ₃ .3H ₂ O and NiCl ₂ .6H ₂ O	50:50	Ethylene glycol	CTAB	10.3
4	IrCl ₃ .3H ₂ O and NiCl ₂ .6H ₂ O	25:75	Ethylene glycol	CTAB	10.1
5	NiCl ₂ .6H ₂ O and IrCl ₃ .3H ₂ O	100 : 0.0	Ethylene glycol	CTAB	59

Table. 3. Synthesis conditions and particle size of Ir-Ni BMNPs with SDS

S. No.	Precursor	Ratio of precursors (%)	Solvent	Surfactant	Approx. particle size in (nm) by XRD
1	IrCl ₃ .3H ₂ O and NiCl ₂ .6H ₂ O	100 : 0.0	Ethylene glycol	SDS	294.6
2	IrCl ₃ .3H ₂ O and NiCl ₂ .6H ₂ O	75:25	Ethylene glycol	SDS	68.3
3	IrCl ₃ .3H ₂ O and NiCl ₂ .6H ₂ O	50:50	Ethylene glycol	SDS	246.2
4	IrCl ₃ .3H ₂ O and NiCl ₂ .6H ₂ O	25:75	Ethylene glycol	SDS	36.6
5	NiCl ₂ .6H ₂ O and IrCl ₃ .3H ₂ O	100 : 0.0	Ethylene glycol	SDS	17.4

Table. 4. Synthesis conditions and particle size of Ir-Ni BMNPs with Tri sodium citrate

S. No.	Precursor	Ratio of precursors (%)	Solvent	Surfactant	Approx. particle size in (nm) by XRD
1	IrCl ₃ .3H ₂ O and NiCl ₂ .6H ₂ O	100 : 0.0	Ethylene glycol	TSC	258.7
2	IrCl ₃ .3H ₂ O and NiCl ₂ .6H ₂ O	75:25	Ethylene glycol	TSC	32.5
3	IrCl ₃ .3H ₂ O and NiCl ₂ .6H ₂ O	50:50	Ethylene glycol	TSC	191.7
4	IrCl ₃ .3H ₂ O and NiCl ₂ .6H ₂ O	25:75	Ethylene glycol	TSC	31.3
5	NiCl ₂ .6H ₂ O and IrCl ₃ .3H ₂ O	100 : 0.0	Ethylene glycol	TSC	14.1

2.4. HR-TEM (High resolution transmission electron microscope)

The high resolution study of the nanoparticles using HRTEM provided further insight into the morphology and size of Ir-Ni BMNPs. HRTEM images obtained are shown in the **Fig. 4(A)** and **4(B)**. The size range of Ir-Ni (3:1)/PVP and Ir-Ni (1:1)/ PVP-BMNPs varies between 1.0-4.2 nm and 1.0-3.5nm as can be seen from the histogram in **Image (i)** and **(ii)** respectively. The approximate size of PVP stabilized Ir-Ni (3:1) and Ir-Ni (1:1) BMNPs is 2.36nm and 1.77nm. Selected area electron diffraction (SAED) is a crystallographic experimental technique that can be performed inside a High resolution transmission electron microscope (HRTEM). Spotty circular rings in **Image (1)** and **(2)** are seen in the SAED pattern which further indicate the crystalline nature and reduced size of the particles.^{39,40} **Fig. 4(a)** demonstrates Ir shell on Ni core of particles while **Fig. 4(b)** shows crystallites arranged in different planes.

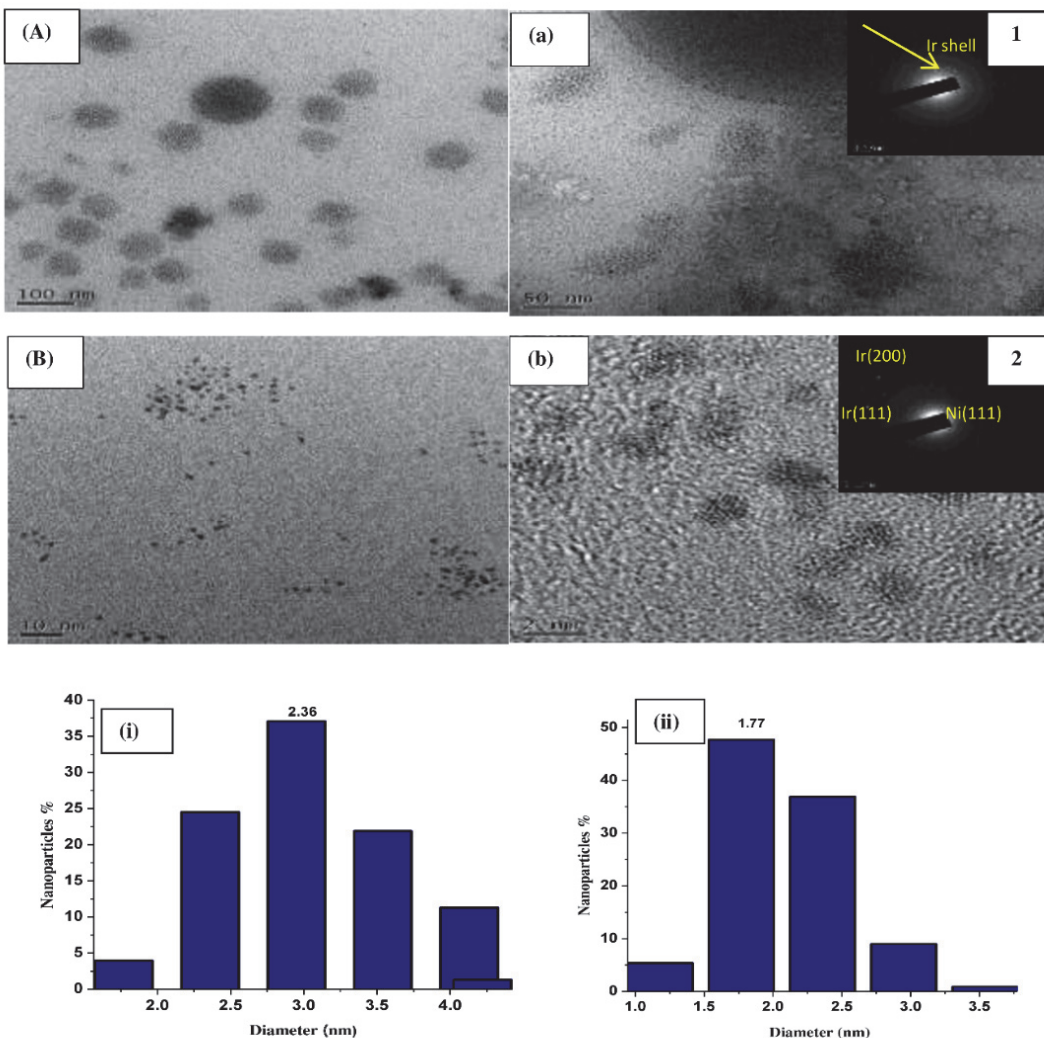


Fig. 4. HRTEM image of PVP stabilized (A) Ir-Ni (3:1) and(B) Ir-Ni (1:1) BMNPs

2.5. FESEM and EDX analysis

In order to analyse the surface structure of the bimetallic nanoparticles Field emission scanning electron microscopy (abbreviated as FESEM) was performed. FESEM images in (**Fig. 5**) show that Ir-Ni (3:1)/PVP-BMNPs consist of polygonal shape aggregates (at high magnification having 6 μm). From **Fig. 5(A)** it is clear that the Ir-Ni (3:1)/PVP-BMNPs nearly have undeviating size and well dispersed in bulk state by avoiding their accretion due to coordination with Ir, Ni ions in the composite mixture.³² From **Fig. 5(B)** it is clear that Ir-Ni (1:1)/PVP-BMNPs are irregular in shape with some agglomeration. Energy dispersive X-ray analysis is a technique that is used to find out the elemental composition. The images of Ir-Ni (3:1)/PVP and Ir-Ni (1:1)/PVP-BMNPs are shown in **Fig. 5(a)** and **5(b)** while the elemental data is shown in **Table 5**. The EDX spectrum in **Fig. 5(a)** and **5(b)** confirms the presence of Ir, Ni, C, and O elements. In **Fig. 5(b)** the presence of Ca, S elements may be due to some minor impurities. The elemental composition percentage ratio of Ir-Ni(3:1) and Ir-Ni (1:1) in **Table 5** are 92:8 and 98:1 respectively. Thus, atomic composition study by EDX analysis indicates that the resultant particles are in core shell structure with Ni core and Ir shell.⁴¹

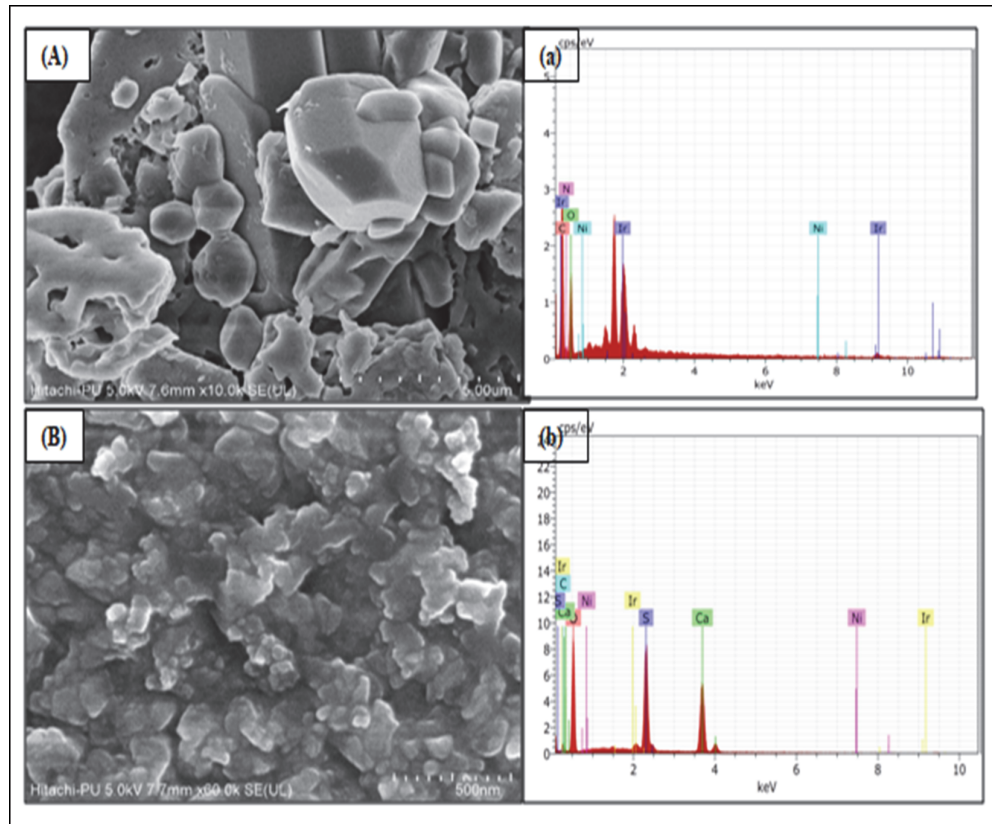


Fig. 5. FESEM images of PVP stabilized (A) Ir-Ni (3:1) BMNPs and (B) Ir-Ni (1:1) BMNPs and EDX images of PVP stabilized (a) Ir-Ni (3:1) and (b) Ir-Ni (1:1) BMNPs

Table 5. EDX analysis of PVP stabilized (A) Ir-Ni (3:1) and (B) Ir-Ni (1:1) ratio BMNPs

Element	Weight % (A)	Atomic % (A)	Weight % (B)	Atomic % (B)
C	42.75	56.82	5.10	8.50
O	31.58	31.50	56.69	71.01
Ir	16.45	1.37	1.19	0.12
Ni	0.23	0.06	0.11	0.04

2.6 Role of surface active agents

Surface active agents are wetting agents that lower the surface tension of a liquid and control the fusion of nanocrystals.^{42,43} To explore the effect of surface active agents on particle size of nanocrystals synthesized by modified polyol process three types of surface active agents PVP (non-ionic), CTAB (cationic), and SDS, TSC (anionic) were used. PVP is considered an excellent stabilizer as it represents favourable protecting qualities owing to its particular structure. It is a homopolymer having a polyvinyl backbone and its repeating units contain highly polar –CONH₂ groups that negotiate hydrophilic and polar attracting qualities, and also having a non polar methylene group both in the backbone and in the ring that negotiate hydrophobic qualities. The N and O in the polar groups have a strong affinity for metal ions and metal nanocrystals.⁴⁴ Calculated particle size of Ir-Ni/surfactants (PVP, CTAB, SDS, and TSC) stabilized BMNPs by XRD is shown in **Tables 1-4**. Ultimate result was found with PVP as size regulator in comparison with CTAB, SDS, and TSC. Size of Ir-Ni (1:1)/PVP BMNPs is 0.8nm and

of CTAB, SDS, and TSC is 10.3nm, 246.2nm, and 191.7nm respectively. There is also a comparison between anionic surfactants SDS and TSC. Although both are anionic surfactants, they can be seen in **Table 3** and **4**. TSC stabilized nanoparticles have smaller particle size in comparison of SDS stabilized nanoparticles. Trisodium citrate works as microreactor for presenting the reaction and a steric surface active agent to inhibit the agglomeration.²³

3. Conclusions

In this study Ir, Ni MNPs and Ir-Ni BMNPs in different ratios (3:1, 1:3, and 1:1) have been successfully synthesized by modified polyol reduction method using different surface active agents such as PVP, CTAB, SDS, and TSC. The addition of surface active agents can affect particle size, coagulation, and flocculation. Therefore, surface active agents play an imperative role in the synthesis of nanoparticles. The synthesized nanoparticles remain more stable and smaller in size with non-ionic surface active agent PVP as compared to CTAB, SDS, and TSC even after several months. X-ray diffraction studies verify that the BMNPs are FCC and amorphous in nature. FTIR corresponds to the interaction between surface active agents and nanoparticles. HRTEM studies reveal that Ir-Ni (3:1)/PVP and Ir-Ni (1:1)/PVP-BMNPs are small in size and less dispersed. Particle size range of these nanoparticles is from (1.77-2.36)nm. FESEM images show that nanoparticles are in quasi spherical shape. Atomic composition studies by EDX analysis indicate that the resultant particles are core shell structure with Ni core and Ir shell. Thus PVP supported Ir-Ni (1:1) BMNPs are small in size 1.77nm less dispersed and amorphous in nature. Therefore, as-synthesized Ir-Ni/ Surfactant supported BMNPs may provide a stable platform for the development of heterogeneous catalysis, green chemistry, and environmentally benign protocol in the near future.

Acknowledgements

The authors are grateful to Gurukul Kangri University, Haridwar for providing the basic facilities for this research work. The authors are also thankful to IIT, Roorkee for XRD analysis, IIT, Bombay for HRTEM analysis and Panjab University Chandigarh for FESEM and FTIR analysis.

4. Experimental

4.1. Materials

All chemicals were achieved from usual profitable sources and used without further analysis. Iridium trichloride trihydrate ($\text{IrCl}_3 \cdot 3\text{H}_2\text{O}$), nickel chloride hexahydrate ($\text{NiCl}_2 \cdot 6\text{H}_2\text{O}$) (used as precursor salt) and ethane-1,2-diol ($\text{C}_2\text{H}_6\text{O}_2$) (used as solvent and reductant) were purchased from SRL. Sodium hydroxide (NaOH) pellets were obtained from Merck. PVP, CTAB, SDS, and TSC, (used as capping agents) were purchased from SRL. Double distilled water was used to prepare all solution.

4.2. Equipments

UV-Vis spectra were recorded using systronic Double-beam spectrophotometer -2203 in the range of 220-800. The samples were in the liquid state and quartz cuvettes having an optical path length of 1.00cm. The Fourier transform infrared (FT-IR) spectra were measured with FTIR (Perkin Elmer) in the range of 4000-400 cm^{-1} using the KBr Pellet technique. The X-ray diffraction (XRD) measurements were performed by using on the dry powders using Bruker Axis D-8 Advance diffractometer with $\text{CuK}\alpha$ ($\lambda = 0.154$ nm) radiation over a range of 2 θ angles from 20-90°. High resolution transmission electron microscope (HRTEM) were performed using (HRTEM 200kv JEM 2100F), operate at an accelerating voltage of 20-200kv. Samples for HRTEM analysis were obtained by using dilute solution of nanocrystals. Field emission electron microscope (JSM 6100 JEOL) SEM was used for surface morphology and shape of nanocrystals.

4.3. Synthesis of monometallic and bimetallic nanocrystals

In the present work, synthesis of Ir, Ni monometallic and Ir-Ni bimetallic nanocrystals in peculiar ratios (3:1, 1:3, and 1:1) using precursor salts of iridium trichloride and nickel chloride by modified polyol reduction method was carried out. To monitor the progression of the nanocrystals formation UV-Visible double beam spectrophotometer is used. A constant peak in the spectrum is the gesture of formation of stable monometallic and bimetallic nanocrystals. Polymer stabilized bimetallic nanocrystals in alcohol were prepared by concurrent reduction of the two corresponding metal salts. Precursor salts of iridium trichloride (0.0059g) and nickel chloride (0.0059g) in disparate ratios were dissolved in 25ml ethylene glycol. A certain amount of one of the surfactant (PVP, CTAB, SDS, and TSC) was added to this solution and the system was stirred at magnetic stirrer until total dissociation of surfactant occurs. To maintain pH sufficient amount of NaOH is added. After being stirred at room temperature the total content was delivered into tri-neck flask and reflux for 3hrs in oil bath at 140°C-180°C temperature. After refluxing the color of the solution changes from pale yellow to blackish brown.

References

- 1 Sharma G., Kumar A., Sharma S., Naushad M., Dwivedi R. P., AL Othman Z. A., and Mola G. T. (2019) Novel development of nanoparticles to bimetallic nanoparticles and their composites: a review. *J. King Saud Univ. Sci.*, 31 (2) 257-269.
- 2 Tejamaya M., Römer I., Merrifield R. C., and Lead J. R. (2012) Stability of citrate, PVP, and PEG coated silver nanoparticles in ecotoxicology media. *Environ. Sci. Technol.*, 46 (13) 7011-7017.
- 3 Li Y., Boone E., and El-Sayed M. A. (2002) Size effects of PVP-Pd nanoparticles on the catalytic Suzuki reactions in aqueous solution. *Langmuir*, 18 (12) 4921-4925.
- 4 Singh S. B. (2016) Iridium chemistry and its catalytic applications: a brief review. *Green Chem. Technol. Lett.*, 2 (4) 206-210.
- 5 Liu Z., and Sadler P. J. (2014) Organoiridium complexes: anticancer agents and catalysts. *Acc. Chem. Res.*, 47 (4) 1174-1185.
- 6 Stowell C. A., and Korgel B. A. (2005) Iridium nanocrystals synthesis and surface coating-dependent catalytic activity. *Nano Lett.*, 5 (7) 1203-1207.
- 7 Islam F., Hossain M. A., Shah N. M., Barua H. T., Kabir M. A., Khan M. J., and Mullick R. (2015) Synthesis, characterization, and antimicrobial activity studies of Ni(II) complex with pyridine as a ligand. *J. Chem.*, 2015.
- 8 Xue H. A. N., Wei C. H. U., Ping N. I., Shi-zhong LUO, and Tao Z..(2007) Promoting effects of iridium on nickel based catalyst in ammonia decomposition. *J. Fuel Chem. Technol.*, 35 (6) 691-695.
- 9 Kalwar N. H., Sirajuddin., Soomro R. A., Sherazi S. T. H., Hallam K. R., and Khaskheli A. R. (2014) Synthesis and characterization of highly efficient nickel nanocatalysts and their use in degradation of organic dyes. *Int. J. Met.*, 2014.
- 10 Egeberg A., Dietrich C., Kind C., Popescu R., Gerthsen D., Behrens S., and Feldmann C. (2017) Bimetallic NiIr₄ and NiOs₄ alloy nanoparticles and their catalytic performance in hydrogenation reactions. *Chem. Cat. Chem.*, 9 (18) 3534-3543.
- 11 Garcia-Gutierrez D. I., Gutierrez-Wing C. E., Giovanetti L., Ramallo-Lopez J. M., Requejo F. G., and Jose-Yacaman M. (2005) Temperature effect on the synthesis of Au-Pt bimetallic nanoparticles. *J. Phys. Chem. B.*, 109 (9) 3813-3821.
- 12 An K., and Somorjai G. A. (2015) Nanocatalyst I: synthesis of metal and bimetallic nanoparticles and porous oxides and their catalytic reaction studies. *Catal. Lett.*, 145 (1) 233-248.
- 13 Kim T., Kabayashi K., and Nagai M. (2007) Preparation and characterization of platinum-ruthenium bimetallic nanoparticles using reverse microemulsions for fuel cell catalyst. *J. Oleo Sci.*, 56 (10) 553-562.

- 14 Singh H. P., Gupta N., Sharma S. K., and Sharma R. K. (2013) Synthesis of bimetallic Pt-Cu nanoparticles and their application in the reduction of rhodamine B. *Colloids Surf. A: Physicochem. Eng. Asp.*, 416 43-50.
- 15 Duan M., Jiang L., Zeng G., Wang D., Tang W., Liang J., Wang H., He D., Liu Z., and Tang L. (2020) Bimetallic nanoparticles/metal-organic frameworks: synthesis, applications and challenges. *Appl. Mater. Today.*, 19 100564.
- 16 Ashraf M. A., Peng W., Zare Y., and Rhee K. Y. (2018) Effects of size and aggregation/agglomeration of nanoparticles on the interfacial/interphase properties and tensile strength of polymer nanocomposites. *Nanoscale Res. Lett.*, 13 (1) 214.
- 17 Wang W., Gu B., and Liang L. (2004) Effect of surfactants on the formation, morphology, and surface property of synthesized SiO₂ nanoparticles. *J. Disper. Sci. Technol.*, 25 (5) 593-601.
- 18 Al-Thabaiti S.A., Malik M. A., Al-Youbi A. A., Khan Z., and Hussain J. I. (2013) Effects of surfactant and polymer on the morphology of advanced nanomaterials in aqueous solution. *Int. J. Electrochem. Sci.*, 8 (1) 204-218.
- 19 Morsy S. M. (2014) Role of surfactants in nanotechnology and their applications. *Int. J. Curr. Microbiol. App. Sci.*, 3 (5) 237-260.
- 20 Simoes M., Pereira M. O., and Vieira M. J. (2005) Action of a cationic surfactant on the activity and removal of bacterial biofilms formed under different flow regimes. *Water Res.*, 39 (2-3) 478-486.
- 21 Tiwari S., Mall C., and Solanki P. P. (2018) Surfactant and its applications: a review. *Int. J. Eng. Res. Appl.*, 8 (9) 61-66.
- 22 Arslan A., Topkaya E., Bingol D., and Veli S. (2018) Removal of anionic surfactant sodium dodecyl sulfate from aqueous solutions by O₃/UV/H₂O₂ advanced oxidation process: process optimization with response surface methodology approach. *Sustain. Environ. Res.*, 28 (2) 65-71.
- 23 Thottoli A. K., and Unni A. K. A. (2013) Effect of trisodium citrate concentration on the particle growth of ZnS nanoparticles. *J. nanostruct. Chem.*, 3 (1) 56.
- 24 Al-Harbi L. M., Kosa S. A., Baloch M. K., Bhatti Q. A., and El-Mossalamy E. S. E. B. H. (2016) Adsorption of polyvinylpyrrolidone over the silica surface: as affected by pretreatment of adsorbent and molar mass of polymer adsorbate. *Int. J. Polym. Sci.*, 2016.
- 25 Shukla M., and Sinha I. (2018) Catalytic Activation of PVP-stabilized gold/silver cluster on p-nitrophenol reduction: a DFT. *Density Functional Calculations –Recent Progresses of Theory and Application*, 153.
- 26 Yue H., Zhao Y., Ma X., and Gong J. (2012) Ethylene glycol: properties, synthesis, and applications. *Chem. Soc. Rev.*, 41 (11) 4218-4244.
- 27 Dong Y. Y., Liu S., Meng L. Y., Wang B., Bian J., and Ma M. G. (2016) An efficient ultrasonic-assisted synthesis of Ag@AgCl@cellulose composites in ethylene glycol solvent. *Mater. Lett.*, 165 210-213.
- 28 Goel A., and Bhatt R. (2012) Synthesis and characterization of nanoscale colloidal iridium metal clusters by chemical reduction method using monohydric and dihydric alcohols. *Int. J. Chem. Appl.*, 4 (2) 111-121.
- 29 Sujata J., Asokan S., and Kumar S. R. (2017) Antioxidant effect and phytochemical analysis of chloroform extract of cassia fistula using FT-IR, HPLC and GC-MS analysis. *Int. J. Pharm. Sci. Rev. Res.*, 46 (1) 129-133.
- 30 Goel A., and Lasyal R. (2018) Facile synthesis of IrO₂ nanoclusters and their application as catalysts in the degradation of azo dyes. *Turk. J. Chem.*, 42 941 – 957.
- 31 Goel A., and Sharma S. (2012) Colloidal iridium nanoparticles in the oxidation of hexacyanoferrate(III) in alkaline medium - a kinetic study. *J. Indian Chem. Soc.*, 89 (4) 507-512.
- 32 Goel A., and Chaudhary M. (2018) Highly dispersed PVP-supported Ir-Ni bimetallic nanoparticles as high performance catalyst for degradation of metanil yellow. *Bull. Mater. Sci.*, 41 (3) 81.
- 33 Roy K., Sarkar C. K., and Ghosh C. K. (2015) Photocatalytic activity of biogenic silver nanoparticles synthesized using yeast (*saccharomyces cerevisiae*) extract. *Appl. Nanosci.*, 5 953-959.
- 34 Saffari J., Mir N., Ghanbari D., Khandan-Barani K., Hassanabadi A., and Hosseini-Tabatabaei M. R. (2015) Sonochemical synthesis of Fe₃O₄/ZnO magnetic nanocomposites and their application in

- photocatalytic degradation of various organic dyes. *J.Mater. Sci: Mater. Electron.*, 26 (12) 9591-9599.
- 35 Mahmoud S. A., Al-Shomar S. M., and Akl A. A. (2010) Electrical characteristics and nanocrystalline formation of sprayed iridium oxide thin films. *Adv. Condens. Matter Phys.*, 2010.
- 36 Kundu S., and Liang H. (2011) Shape-selective formation and characterization of catalytically active iridium nanoparticle. *J.Colloid Interface Sci.*, 354 (2) 597-606.
- 37 Darabdbara G., Das M. R., Amin M. A., Mersal G. A. M., Mostafa N. Y., Abd El-Rehim S. S., Szunerits S., and Boukherroub R. (2018) Au-Ni Alloy nanoparticles supported on reduced grapheme oxide as highly efficient electrocatalysts for hydrogen evolution and oxygen reduction reactions. *Int. J. Hydrog. Energy.*, 43 (3) 1424-1438.
- 38 Chiang I. C., Chen Y. T., and Chen D. H. (2009) Synthesis of NiAu colloidal nanocrystals with kinetically tunable properties. *J. Alloys Compd.*, 468 (1-2) 237-245.
- 39 Antoinette M. M., and Israel S. (2017) Synthesis and characterization of Sm₂O₃ nanoparticles using combustion method. *Int. Res. J. Eng. Tech.*, 4 276-9.
- 40 Redon R., Ramirez-Crescencio F., and Fernandez-Osorio A. L. (2011) Solventless synthesis of iridium(0) nanoparticles. *J.Nanopart. Res.*, 13 (11) 5959–5965.
- 41 Larios E., Molina Z., Maldonado A., and Tanori J. (2012) Synthesis and characterization of bimetallic copper gold nanoparticles. *J. Disper.Sci.Technol.*, 33 (5) 719-723.
- 42 Mishra M., Muthuprasanna P., Prabha K. S., Rani P. S., Satish I. A., Chandiran I. S., Arunachalam G., and Shalini S. (2009) Basics and potential applications of surfactants-a review. *Int. J. Pharmtech. Res.*, 1 (4) 1354-1365.
- 43 Heinz H., Pramanik C., Heinz O., Ding Y., Mishra R. K., Marchon D., Flatt R. J., Estrela-Lopis I., Llop J., Moya S., and Ziolo R. F. (2017) Nanoparticle decoration with surfactants: molecular interactions assembly and applications. *Surf. Sci. Rep.*, 72 (1) 1-58.
- 44 Malina D., Sobczak-Kupiec A., Wzorek Z., and Kowalski Z. (2012) Silver nanoparticles synthesis with different concentration of polyvinylpyrrolidone. *Dig. J. Nanomater.Bios.*, 7 (4) 1527-1534.



© 2021 by the authors; licensee Growing Science, Canada. This is an open access article distributed under the terms and conditions of the Creative Commons Attribution (CC-BY) license (<http://creativecommons.org/licenses/by/4.0/>).